Available online at www.sciencedirect.com
SCIENCE DIRECT®
Journal of Nuclear Materials 337–339 (2005) 525–529
journal of nuclear materials
www.elsevier.com/locate/jnucmat

Particle control issues of a compact stellarator with external vacuum vessel

Peter Mioduszewski *, the QPS Group

Oak Ridge National Laboratory, P.O. Box 2008, M.S. 6169, Oak Ridge, TN 37831-6169, USA

Abstract

The Quasi-Poloidal Stellarator (QPS) [J.F. Lyon, S.P. Hirshman, D.A. Spong, et al., 30th EPS Conference on Plasma Phys. Control. Fusion, St. Petersburg, 2003] has a very low plasma aspect ratio ($R/a \sim 2.7$) and is a new confinement approach that could ultimately lead to a high-beta compact stellarator reactor. QPS is being developed to test key features of this approach. In QPS, the modular stellarator coils and other components are inside the vacuum vessel, requiring special attention with respect to particle control. We have analyzed two specific aspects: (1) The casings of the internal coils will assume elevated temperatures during operation whereas the vacuum vessel will be at room temperature; we have analyzed the consequences for adsorbed gas layers. (2) The plasma is surrounded by a large gas reservoir that might cause problems for density control. We have constructed a model to predict plasma and neutral densities as functions of fueling, divertor baffling, wall adsorption, and particle exhaust. This model predicts that plasma and neutral densities can be controlled.

PACS: 52.40.Hf
Keywords: Density control; Baffling effect; Particle balance; Particle control

1. Introduction

The Quasi-Poloidal Stellarator (QPS) [1] experiment is being developed to test key features of the compact stellarator confinement approach. The device parameters will be: $R = 0.9\,\text{m}$, $\langle a \rangle = 0.33\,\text{m}$, $B = 1\,\text{T}$, $t = 1\,\text{s}$. The quasi-poloidal symmetry leads to neoclassical transport much lower than anomalous transport. The reduced effective field ripple may also produce reduced poloidal viscosity, enhancing the ambipolar $E \times B$ poloidal drift and allowing larger poloidal flows for reduction of anomalous transport. Compact stellarators could combine the best features of tokamaks and stellarators in a low-aspect-ratio device by using three-dimensional (3-D) shaping of the last closed flux surface, quasi-symmetry features to improve neoclassical transport, and some bootstrap current to provide a fraction of the required rotational transform. A cutaway view of the planned device is depicted in Fig. 1.

QPS is being designed with an external vacuum vessel, i.e. the modular coils and other components are inside the vacuum vessel. This entails large internal surfaces and requires special attention with respect to particle and impurity control. We investigate two specific features of the device. (1) The stainless steel casings

* Corresponding author. Tel.: +1 865 574 2715; fax: +1 865 574 1191.
E-mail address: mioduszewspk@ornl.gov (P. Mioduszewski).

0022-3115/$ - see front matter © 2004 Elsevier B.V. All rights reserved.
doi:10.1016/j.jnucmat.2004.10.024

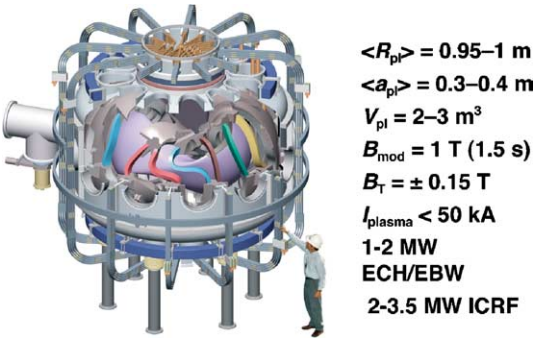

Fig. 1. Cutaway view of the QPS device.

of the internal coils will assume elevated temperatures during operation whereas the vacuum vessel will be at room temperature; we analyze the temperature effects on adsorbed gases. (2) The plasma is surrounded by a large gas reservoir and we evaluate specific measures needed for density control.

2. Effects of temperature and desorption energy on adsorbed gas layers

First, we look at gas adsorption as a function of desorption energies and surface temperatures. The QPS vacuum vessel has a volume of $V = 20\,\mathrm{m}^3$, internal surface $A = 160\,\mathrm{m}^2$, and effective pumping speed $S = 2\,\mathrm{m}^3/\mathrm{s}$ (turbo-molecular pumps) or $20\,\mathrm{m}^3/\mathrm{s}$ (appendage cryo-pumps). The overall particle balance has to include the adsorption/desorption dynamics if there are gas species with binding energies in the range of 50–100 kJ/mole [2]. With the volumetric density n_v, the surface density n_s, the sticking coefficient s, the particle surface sojourn time τ, the external leak rate Q, and the pumping speed S, the balance is given by:

$$V \cdot \frac{\mathrm{d}n_v}{\mathrm{d}t} = A \cdot \frac{n_s}{\tau} + Q - A \cdot s \cdot \frac{n_v \bar{v}}{4} - n_v \cdot S \qquad (1)$$

$$A \cdot \frac{\mathrm{d}n_s}{\mathrm{d}t} = A \cdot s \cdot \frac{n_v \bar{v}}{4} - A \cdot \frac{n_s}{\tau}. \qquad (2)$$

Eq. (1) represents the evolution of the volumetric density and equation (2) that of the surface particle density. The sojourn time τ is a function of the desorption energy and surface temperature, given by the Frenkel equation $\tau = \tau_0 \exp(E/RT)$, with $\tau_0 = 10^{-13}\,\mathrm{s}$, the desorption energy E in kJ, the gas constant $R = 8.3\,\mathrm{J/moleK}$, and the surface temperature T in K [3]. The above system of coupled ordinary differential equations (ODEs) can be solved analytically with standard techniques [4]. Due to space limitation, we show here only the results.

Fig. 2(a) and (b) show the volumetric density $n_v(t)$ and the surface density $n_s(t)$ of the vacuum vessel as a function of time, including the external leak rate of $Q = 10^{-5}\,\mathrm{Torr\,L/s}$ or 3.5×10^{14} particles/s. Eqs. (1) and (2) are solved for three different desorption energies: 91, 71, and 54 kJ/mole, typical for H_2O, CO, and H_2 respectively on stainless steel [5]. The sticking coefficient is taken as $s = 0.05$.

Fig. 2(a) shows the pump-out of the vacuum vessel for H_2O with a desorption energy of 91 kJ/mole. We see that for $T = 293\,\mathrm{K}$, the surface and volume densities do not change over the period shown in the plot. The densities remain at the initial values and the system is controlled by adsorption/desorption processes (we assume multi-molecular layers). As the temperature is increased to $T = 373\,\mathrm{K}$, the densities decay slowly due to pumping, but are still mostly controlled by the adsorption/desorption equilibrium. The surface density is now at $n_s = 10^{15}\,\mathrm{m}^{-2}$, or <0.001 monolayers, i.e. for high binding energies, elevated temperatures have a strong effect on the surface coverage.

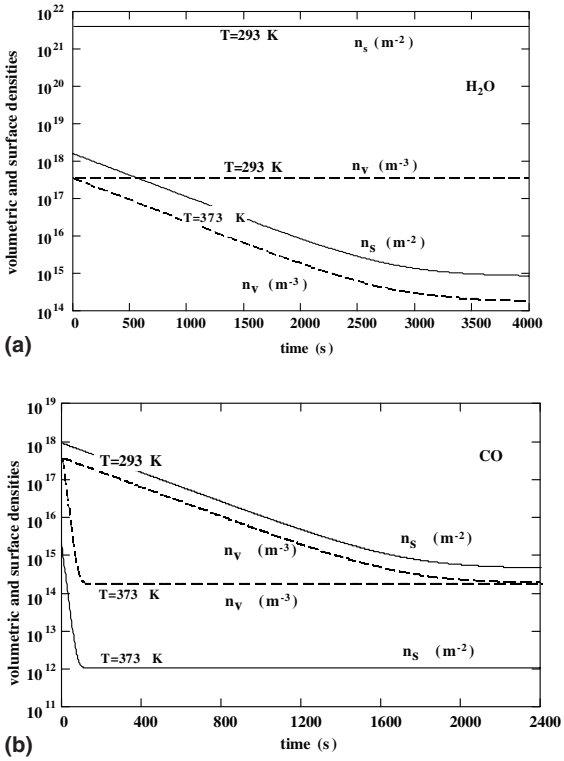

Fig. 2. (a) Pump-out of H_2O with $E = 91\,\mathrm{kJ/mole}$. At the lower temperature the wall has a high coverage and the particle dynamics is controlled by the adsorption/desorption equilibrium. At the elevated temperature, pumping comes into play. (b) Pump-out of CO with $E = 71\,\mathrm{kJ/mole}$. At the lower temperature the particle dynamics is still mostly controlled by the surface equilibrium, whereas for $T = 373\,\mathrm{K}$ the dynamics is controlled by the pumping time constant.

In Fig. 2(b) we see the effect of the surface temperature on CO (71 kJ/mole). Even at room temperature, the equilibrium is reached in a time much shorter than in the previous case and at $T = 373$ K, the equilibrium densities are reached very quickly and the surface coverages become negligibly small. For the low desorption energy of H_2, the pump-out dynamics is entirely determined by volumetric pumping, even at room temperature. Due to space limitation, this example is not shown here.

Overall, the analysis shows the effect of surface temperatures on the dynamics of pumping, including adsorbed gas layers. At room temperature, species with low and high binding energies do not affect the pump-down dynamics, because they are either desorbed very fast or not at all. However, for plasma impurity control, the high binding energies are relevant, since plasma-induced desorption can release species with binding energies much higher than those considered here.

Next, we analyze a case with the plasma-facing components at higher temperature then the surrounding vessel. Now we have three coupled ODEs and the algebra involved in analytic solutions becomes tedious. Hence, we use a numerical (Runge-Kutta) solver for the balance equations:

$$V \cdot \frac{\mathrm{d}n_\mathrm{v}}{\mathrm{d}t} = A_1 \cdot \frac{n_{\mathrm{s}1}}{\tau_1} + A_2 \cdot \frac{n_{\mathrm{s}2}}{\tau_2} + Q - \left(A_1 \cdot \frac{s \cdot \bar{v}_1}{4} + A_2 \cdot \frac{s \cdot \bar{v}_2}{4} + S \right) \cdot n_\mathrm{v}, \tag{3}$$

$$A_1 \cdot \frac{\mathrm{d}n_{\mathrm{s}1}}{\mathrm{d}t} = A_1 \cdot s \cdot \frac{n_\mathrm{v} \bar{v}_1}{4} - A_1 \cdot \frac{n_{\mathrm{s}1}}{\tau_1}, \tag{4}$$

$$A_2 \cdot \frac{\mathrm{d}n_{\mathrm{s}2}}{\mathrm{d}t} = A_2 \cdot s \cdot \frac{n_\mathrm{v} \bar{v}_2}{4} - A_2 \cdot \frac{n_{\mathrm{s}2}}{\tau_2}. \tag{5}$$

Eqs. ()()()(3)–(5) describe particle densities in the volume V, and on the surfaces A_1 and A_2. For the initial values, we assume a volume density of $n_\mathrm{v} = 3.5 \times 10^{17}\,\mathrm{m}^{-3}$ and the surface densities (for $i = 1,2$) are calculated from the equilibrium equations for $\mathrm{d}n_{si}/\mathrm{d}t = 0$, i.e. $n_{si} = \tau_i \cdot s(n_\mathrm{v}\, \mathrm{v}_i/4)$. Fig. 3(a) shows surface and volumetric densities for CO with surfaces at $T = 293$ K and 373 K. The coverage on the hotter surface is almost three orders of magnitude lower. However, comparing with Fig. 2(b), we find that the pump-out dynamics is mostly controlled by the colder surface.

For H_2O the 'pump-out' is shown in Fig. 3(b) with surface temperatures $T = 293$ K and 373 K. Over the period shown, there is no pump-out and all densities remain constant. This is in contrast to Fig. 2(a), where we do see an effect at $T = 373$ K. The difference is that in Fig. 3(b), the pump-out dynamics is controlled by the colder surface, corresponding to the $T = 293$ K case of Fig. 2(a). However, the surface coverage at elevated temperature is several orders of magnitude lower, i.e. more favorable for minimizing plasma contamination. Finally, for H_2 the surface coverage is so low that the particle dynamics is totally determined by volumetric pumping. Again, this example is not shown here.

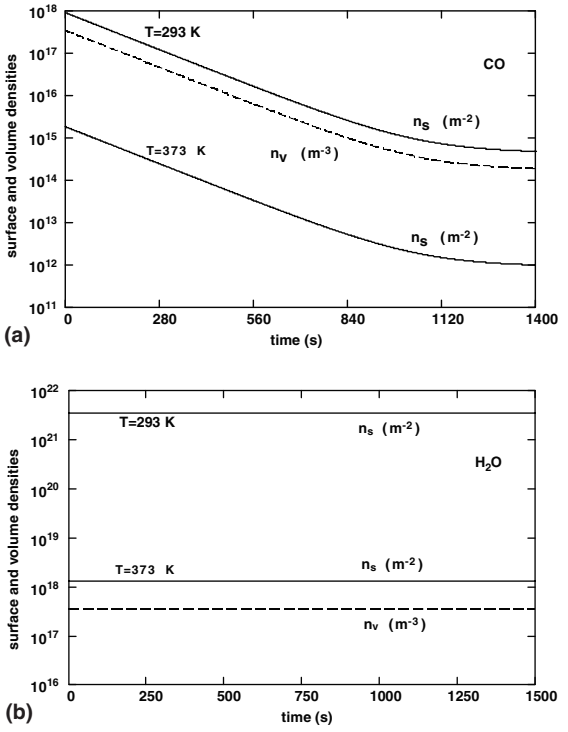

Fig. 3. (a) Pump-out of CO with $E = 71$ kJ/mole with inner and outer surfaces at different temperatures: $T = 293$ K for the outer and 373 K for the inner surface. The dynamics is a mixture of surface equilibrium and vacuum pumping. (b) 'Pump-out' of H_2O with $E = 91$ kJ/mole with outer and inner surfaces at $T = 293$ K and 373 K respectively. In this case, the particle dynamics is totally controlled by the colder surface.

In conclusion, for species with medium and high binding energies, it is advantageous for impurity control to have the coil casings and structural shell at higher temperature than the vacuum vessel, even though the pump-out dynamics is controlled by the colder surface.

3. Density control

With an external vacuum vessel measuring ten times the plasma volume, special measures are necessary for plasma density control. In order to identify the controlling parameters, we evaluate the overall particle balance. With the subscripts p, g, and w for plasma, gas, and wall, the particle balance is given by the following equations:

$$V_\mathrm{p} \frac{\mathrm{d}n_\mathrm{p}}{\mathrm{d}t} = \eta\phi(t) - \frac{n_\mathrm{p} V_\mathrm{p}}{\tau}(1 - \alpha R) + A_\mathrm{p} \frac{n_\mathrm{g} v_\mathrm{g}}{4} \beta_\mathrm{FC} \beta_\mathrm{ion}, \tag{6}$$

$$V_g \frac{dn_g}{dt} = (1-\eta)\phi(t) + \frac{n_p V_p}{\tau}(1-\alpha)R - A_p \frac{n_g v_g}{4}\beta_{FC}\beta_{ion} - n_g S, \quad (7)$$

$$V_w \frac{dn_w}{dt} = \frac{n_p V_p}{\tau}(1-R), \quad (8)$$

for the plasma density n_p, the gas density n_g, and the surface particle density n_w respectively, with ϕ (t) the fueling rate, η the fueling efficiency, τ the particle confinement time, R the divertor recycling coefficient, α the recycling efficiency, i.e. the fraction of the recycling flux that gets back into the plasma, and β_{FC} and β_{ion} the efficiencies for Franck–Condon effect and ionization of particles in the surrounding gas.

In the first example we use $\tau = 0.1\,s$, $R = 0.9$, and $S = 2\,m^3/s$. The gas puff is tailored for a quick rise, followed by a flat-top, and puffed into the vessel, corresponding to a low (assumed) fueling efficiency $\eta = 0.05$. The divertor is not baffled, corresponding to a low (assumed) recycling efficiency $\alpha = 0.5$. The ionization probability of the gas surrounding the plasma is $\gamma = \beta_{FC}\,\beta_{ion}$; the result turns out not to be very sensitive to γ (we use $\gamma = 0.5$). For a plasma volume of $2\,m^3$, a gas volume of $20\,m^3$, a divertor surface area of $1\,m^2$, and a gas puff as shown in Fig. 4(a), we obtain the plasma density evolution shown in Fig. 4(a). Due to the low fueling efficiency, the gas density builds up first and the plasma is subsequently fuelled by the surrounding gas. The plasma density ends up being about half the surrounding gas density.

Neutral densities higher than the plasma density are not desirable and we try to remedy this by placing the gas puff nozzle at the divertor plate, puffing directly into the plasma. This case would correspond to a high fueling efficiency, e.g. $\eta = 0.9$. With all other parameters as before, the result is shown in Fig. 4(b). The plasma density builds up faster than the gas density and remains about constant after the initial rise. This is a clear improvement over the first scenario, although, due to the poor baffling at the divertor, neutral gas still builds up and eventually reaches the plasma density level.

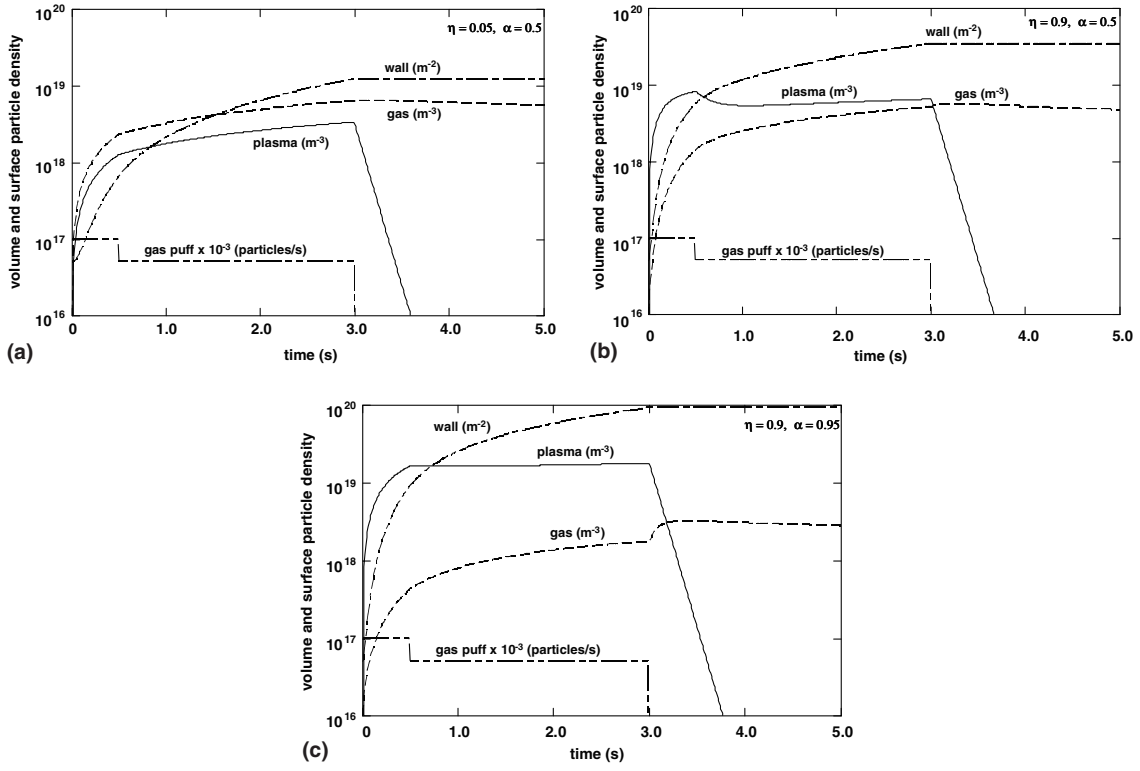

Fig. 4. (a) Particle densities as a function of time. Fueling efficiency is $\eta = 0.05$ and divertor baffling efficiency is $\alpha = 0.5$. Gas puff is in 1/1000 particles/s. The neutral gas density builds up first and then the plasma is fuelled by the surrounding gas. The gas density is twice as high as the plasma density. (b) Particle densities as a function of time with high fueling efficiency $\eta = 0.9$ and low divertor baffling efficiency $\alpha = 0.5$. Due to the high fueling efficiency the plasma builds up first and the gas follows, but the low divertor baffling efficiency causes the gas to build up eventually to the value of the plasma density. (c) Particle densities as a function of time with $\eta = 0.9$ and $\alpha = 0.95$. High fueling and baffling efficiencies lead to fast plasma build-up and slow increase of the gas density.

For further improvement, we introduce tight baffling at the divertor and take this into account by setting $\alpha = 0.95$. This leads to the desired result shown in Fig. 4(c): the plasma density rises fast and then remains constant, and the gas density is at least an order of magnitude lower. At the end of the discharge, the collapsing plasma contributes to the gas density.

4. Summary

The QPS compact stellarator is being designed with an external vacuum vessel and needs special attention with respect to particle and impurity control. We have analyzed the particle balance between residual gases and surface adsorbates for a vessel with surfaces at two different temperatures. The surface coverage of gases with medium and high desorption energies can be drastically reduced by elevated temperatures, whereas the pump-out dynamics is determined by the colder temperature of the vacuum vessel. For low desorption energies, the surface coverage is very low, even at room temperature, and the pump-out dynamics are completely controlled by the pumping time constant.

For density control, a systematic variation of the parameters in our model shows the following results: The gas puff determines the absolute values of plasma and gas densities, but not the relative levels. The recycling coefficient R controls the wall inventory and the absolute values of plasma and gas, but does not affect the ratio of the two. The ionization efficiency γ of the surrounding gas has a relatively small effect. The plasma density is roughly proportional to the particle confinement time. The pumping speed S has a clear effect on the neutral gas: increasing it from $2\,m^3/s$ to $20\,m^3/s$ (with appendage cryo-pumps), decreases the gas density by a factor 2.5, but the plasma density only by about 10%. The two 'knobs' that have the strongest effect on controlling plasma versus gas density are the fueling efficiency η and the recycling efficiency α. With these two parameters, we should be able to control plasma and neutral densities as shown. Neutral densities of similar levels as obtained here were no obstacle for achieving high plasma performance in current stellarators [6]

Acknowledgment

This work was sponsored by the Office of Fusion Energy Sciences, US Department of Energy, under contract DE-AC05-00OR22725 with UT-Battelle, LLC.

References

[1] J.F. Lyon, S.P. Hirshman, D.A. Spong, et al., 30th EPS Conference on Plasma Phys. Control. Fusion, St. Petersburg, 2003.
[2] G. Lewin, Fundamentals of Vacuum Science and Technology, McGraw Hill, 1965.
[3] P.A. Redhead, J.P. Hobson, E.V. Kornelsen, The Physical Basis of Ultra-High Vacuum, Chapman and Hall, 1968.
[4] E. Kamke, Gewohnliche Differentialgleichungen, Chelsea Publ. Company, 1959.
[5] Y. Strausser, Review of Outgassing Results, Varian Report VR-51, 1968.
[6] P. Grigull, K. McCormick, J. Baldzuhn, et al., Plasma Phys. Control. Fusion 43 (2001) A175.